ORIGINAL PAPER

Adsorption performance and thermodynamic analysis of SAPO-34 silicone composite foams for adsorption heat pump applications

L. Calabrese[1,3] · L. Bonaccorsi[2] · P. Bruzzaniti[1] · A. Frazzica[3] · A. Freni[4] · E. Proverbio[1]

Abstract

In the present work, adsorption performances of an innovative composite adsorber, based on SAPO-34-silicone composite macro-cellular foams, are reported. The choice of a foamed structure was assessed to improve the water vapor access towards the embedded zeolite keeping good adsorption heat pump dynamic performance. Depending on zeolite amount used as filler, zeolite/silicone foams evidenced a soft and open cell configuration (low zeolite content) or rigid and closed one (high zeolite content). Morphological analysis evidenced that the cellular structure of the foam is homogeneous and well distributed along the foam cross section. Adsorption tests showed that the adsorbent foamed samples have very effective adsorption capabilities indicating that the porous structure of the filled pure zeolite was not obstructed. SAPO-34 filler contributed actively, with an efficiency above 90%, to the adsorption performances of the composite foam. Starting from experimental equilibrium data, a simple thermodynamic analysis based on energy balances was carried out for air conditioning application. Results of the analysis demonstrated that foam technology can guarantee cooling COP up to 7% higher than that estimated for the typical adsorber solution based on loose adsorbent grains inside an aluminum finned-flat tube heat exchanger, which is very promising for practical application in adsorption heat pumps.

Keywords Adsorption heat pump · Zeolite · Composite foam · Silicone · Adsorption performances

Introduction

Adsorption Heat Pumps (AHP) use environmental friendly refrigerants (e.g., water) and can be driven by waste heat or solar energy, thus reducing emissions and fuel consumption associated with air conditioning systems of automotive, industrial and residential sectors [1]. Recent R&D activities have been focused on the development of efficient, reliable and lightweight AHP units, in order to make this technology fully competitive with conventional vapor compression systems [2, 3]. The adsorbent material is the core component of an AHP, enabling the sorption thermodynamic cycle. Nowadays, silico-alumino-phosphates zeo-types (SAPO, AlPO) and silica gel are considered the state-of-art adsorbent materials for application in AHP [4, 5], especially in terms of low regeneration temperature ($T_{reg} < 100$ °C), favorable S-shaped isotherm and proved mechanical and hydrothermal stabilities [6]. Recent studies reported metal-organic frameworks (MOFs) [7], composites "salt confined into a matrix" [8] and dealuminated Y zeolites [9] as promising class of materials, however, still at early stage of development [10]. Additionally, the performance of an AHP is related not only to the basic adsorption properties of the adsorbent materials but also to the heat and mass transfer properties of the adsorbent bed and related operating conditions. Ideally, an improved adsorbent bed should guarantee the following: to increase the sorption capacity; to limit the vapor pressure drop; to reduce the component size and cost [11]. Accordingly, there is an increasing effort in developing new heat exchange concepts and adsorbent heat exchangers that meet such requirements [3]. Many studies on the subject focused on the development of coated adsorbent exchanges, in which the direct application of the adsorbent coating reduces the

✉ L. Calabrese
lcalabrese@unime.it

1 Department of Engineering, University of Messina, Contrada di Dio Sant'Agata, 98166 Messina, Italy

2 Department of Civil Engineering, Energy, Environment and Materials, University Mediterranea of Reggio Calabria, Salita Melissari, 89124 Reggio Calabria, Italy

3 CNR ITAE, Salita Santa Lucia Sopra Contesse 5, 98126 Messina, Italy

4 CNR-ICCOM, Via G. Moruzzi 1, 56124 Pisa, Italy

Springer

contact resistance between the heat exchanger and the adsorbent itself. In the literature, most potentially effective coating methods are direct zeolite synthesis [12–15] and binder-based coating depositions [16–18]. Direct synthesis of a pure zeolite layers on a metal substrate allows nearly perfect adhesion. However, the process is complex and the achievable zeolite layer thickness is too limited (< 0.1 mm). The binder-based coating method can be easily implemented by spray or dip-coating technique and offers the possibility to vary coating thickness in the range 0.1–0.5 mm by controlling the formulation parameters. Recently, efficient organic and silane-based coating techniques have been developed [19, 20] and full-scale coated adsorbers were experimentally tested in [16], showing promising performance as power density. However, coating is usually characterized by poor mechanical strength that favors easy loss of zeolite particles from the metal supports upon repeated temperature swings, due to the difference in their thermal expansion coefficients [18]. A draw-back of this route is the low zeolite content in the adsorber, caused by the thin coating thickness, that allows, therefore, low adsorbent density (usually in the range 150–300 g/dm^3). Furthermore, the coated adsorber systems are characterized by low ratio between the heat capacity of the adsorbent material and that one of the metallic heat exchanger (typically 0.2–0.3), thus significantly affecting the AHP performance (mainly related to mass transport effects to and from the layers, especially on completely filling in the fin space of the coated heat exchanger with the adsorbent).

On this concern, a suitable approach could be to increase adsorbent surface area with minimized gas flow pressure losses and diffusion resistance generating a macro-porous structure embedded in heat exchanger component. A possible solution is to realize a zeolite foamed composite materials with well-interconnected porous structure for easier internal molecular diffusion [21–24].

Composite macro-cellular foams, due to their high surface area, are able to have a large content of adsorbent zeolite materials per unit volume, the foam porosity behaving also as preferential paths for the water vapor diffusion. This method guarantees a higher adsorbent zeolite content in the adsorber, even if at the same time it adds an additional passive mass in the adsorber component that can reduce the adsorption heat pump performance. Recently, Bonaccorsi et al. [25] investigated a low weight graphite foamed structure as support to allow the growth by direct synthesis of an SAPO-34 zeolite coating for adsorption chillers obtaining promising results.

More recently, a new composite zeolite foam based on silicone matrix was synthesized for application in adsorption heat pumps [26, 27]. The purpose was to obtain an adsorbent zeolite-based macro-porous composite structure with relevant advantages on several aspects such as synthesis process, low density, high vapor diffusion permeability and

good hydrothermal and mechanical stability [28]. On the basis of the present knowledge, the development of a heat exchanger based on zeolite foam could be an effective engineering design solution to maximize performance, heat and mass transfer properties and functionality of these systems [29]. The choice of a foamed structure as adsorbent material may enhance the active surface area without altering the AHP dynamic performance.

In the present work, adsorption performance and thermodynamic analysis of an innovative composite adsorber, based on SAPO-34 filled silicone foams, were evaluated. Samples at increasing zeolite content, from 40 to 70 wt%, were synthesized. Morphological analysis, performed by scanning electron microscopy (SEM) and 3D optical microscopy, has been applied to assess the relationship between constituents ratio and foam microstructure. Furthermore, water vapor adsorption capabilities were also evaluated using thermogravimetric method using real AHP operating conditions. A key point that was investigated, despite previous research activities [26, 27], is to optimize the adsorption performances of the composite foams taking into account their use in AHP system components. In particular, a thermodynamic analysis was carried out starting from the relationship between adsorption capabilities and foam microstructure.

Specifically, the thermodynamic efficiency, in terms of cooling COP, of an adsorber component constituted by the proposed foam compositions was calculated against the conventional loose adsorbent grains inside an aluminum finned-flat tube heat exchanger (HEX), in order to assess the potential of the real applicability of this class of materials for AHP systems.

Experimental part

Zeolite synthesis

Zeolite SAPO-34 was synthesized under hydrothermal condition, according to the procedure reported in [2]. The zeolite is obtained as crystalline powder made of particles with the typical cubic shape and average size in the range of 2–5 μm. Then, the zeolite was calcined at 550 °C for 6 h under continuous airflow to remove the template. The crystalline structure of synthesized SAPO-34 powder was verified by X-Ray diffraction (Bruker D-8 Advance, Cuka, 40 kV–40 mA).

Foam synthesis

Zeolite–silicone composite foams were realized following an open to air mold foaming technique. The system was made up by two reactants (both supplied by Gelest Inc., Morrisville, USA): a Poly(dimethylsiloxane-co-methylhydrosiloxane),

trimethylsilyl terminated, PMHS, M.W. 5500–6500 CAS: 68037-59-2 and a silanol terminated polydimethylsiloxane, PDMS, M.W. 110,0000 CAS: 70131-67-8 compounds containing Tin(II) 2-ethylhexanoate [Sn(II)] d:1.12, M.W. 405.11, 50%, CAS. 301-10-0 as catalyst. Specifically, the foam synthesis was performed as in the following: pure SAPO-34 filler (Si/Al ratio 0.18) was mixed in polydimethylsiloxane (PDMS) for about 60 s. The solution was reduced adding water and ethanol solvents. Afterwards, the polymethylhydrosiloxane (PMHS) was added with the zeolite/PDMS mixture (employing a PDMS/PMHS compound ratio 1:2) and thoroughly mixed for 15 s. Finally, the tin catalyst was added under vigorous mixing, for about 15 s. The so-obtained mixture was poured into a cylinder mold to allow blowing. Foaming process was activated putting the sample into an oven kept at a controlled temperature (60 °C) for 24 h to obtain a complete compounds reaction. In Fig. 1, the scheme of the composite foam preparation is reported.

$$\equiv Si - OH \; + \; H - Si \equiv \; \rightarrow \; \equiv Si - O - Si \equiv \; + \; H_2 \uparrow \qquad (1)$$
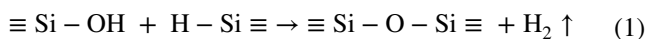
Poly-addition and poly-condensation reactions take place between silanol groups of PDMS and Si–H groups of PMHS [30]. New Si–O-Si covalent bonds, formed thanks to reaction reported in Eq. 1, lead to the formation of a rubber-like polymer network [31]. Gaseous hydrogen product, formed in the crosslinking reaction, induces the foam blowing [32]. Thus, the crosslinking process and the foaming evolve simultaneously during the synthesis. Foams at varying SAPO-34 filler content, in the range 20–70 wt% of siloxane matrix (PDMS + PMHS), were realized. A list of all produced formulations with details of compound amounts and zeolite filler content is reported in Table 1. As reference, an unfilled silicone foam was considered (ZF-0).

Composite foam characterization

Foam adsorption performances were evaluated using a thermogravimetric dynamic vapor system (Surface Measurements Systems DVS Vacuum). The system consists of a micro-balance, with a precision of 0.1 µg on the measured weight, and a water vapor pressure flow control device inside the measuring chamber. Everything is placed inside a temperature controlled box kept at a constant temperature. Water adsorption isobars were measured on about 0.5 cm³ of foamed sample, corresponding to a mass of about 350–500 mg.

Foam morphology and surface characterization were evaluated by optical microscope (Hirox HK-8700) and focused ion beam scanning electron microscope (ZEISS SEM/FIB crossbeam 540). The apparent foam density was calculated using weight to bulk volume ratio.
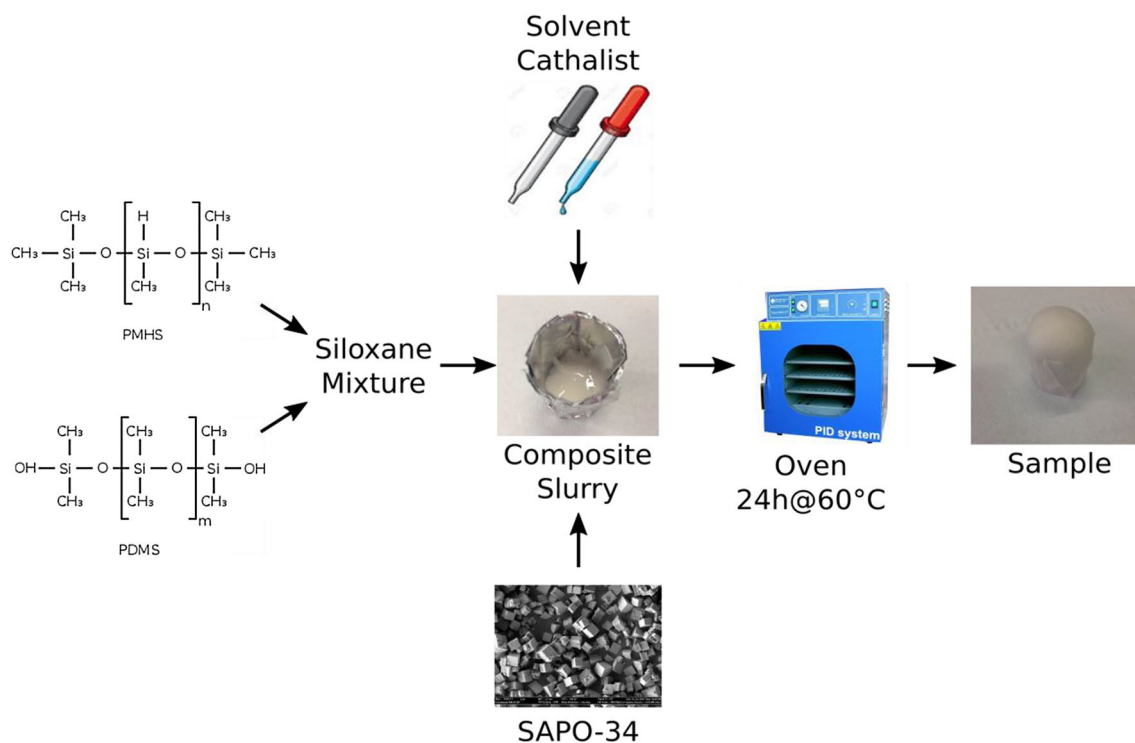

Fig. 1 Scheme of the composite foam preparation

Table 1 Siloxane solution formulations at varying zeolite filler content

|		ZF-0 (%)	ZF-40	ZF-50 (%)	ZF-60 (%)	ZF-66 (%)	ZF-70 (%)
PDMS	Siloxane	42.6	29.4	26.0	21.7	18.7	17.2
PMHS	Siloxane	21.3	14.7	13.0	10.9	9.3	8.6
Ethanol	Solvent	14.9	10.3	9.1	7.6	6.5	6.0
Water	Solvent	10.6	7.4	6.5	5.4	4.7	4.3
Sn(II)	Catalyst	10.6	7.4	6.5	5.4	4.7	4.3
Zeolite	Filler	0.0	30.9	39.0	48.9	56.1	59.5
Zeolite/foam (%)		0.0	40.0	50.0	60.0	66.0	70.0
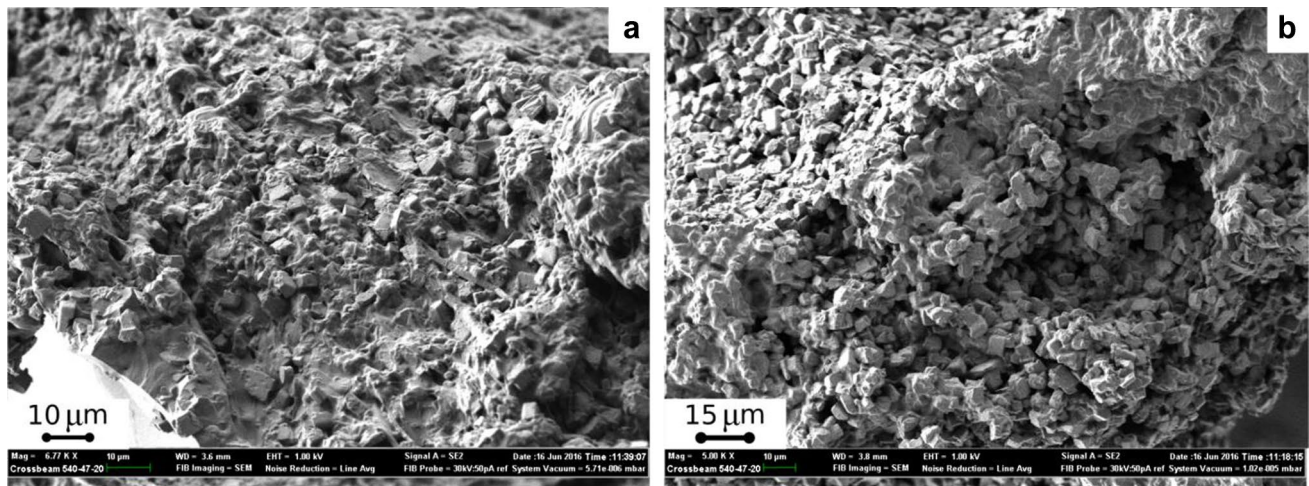
Fig. 2 SEM image of cellular wall in ZF-50 (**a**) and ZF-70 (**b**) foam samples

Results and discussion

Morphological analysis

In Fig. 2, SEM images of fracture surfaces, for ZF-50 and ZF-70 samples, used as reference of low and high SAPO-34 filler content of composite foams, respectively, are reported. Both composite foams show a quite rough morphology with peaks and valleys along the strut cross section. Foam structure is homogeneous and defect-free, evidencing also uniform cellular walls without cracks. Cubic shaped SAPO-34 zeolite crystal (average dimension about 3 μm) is well dispersed and interconnected with the silicone matrix.

Figure 3 shows another SEM image of ZF-70 foam, at higher magnification, in order to highlight the interaction between the zeolite crystals and the matrix. At the zeolite grain/matrix interface, no discontinuities or debonding was observed showing that the filler is embedded and adherent to the matrix. This indicates a good chemical affinity between the composite foams constituents. In fact, the external hydroxyl groups of zeolite grains can chemically interact with reactive terminated groups of the
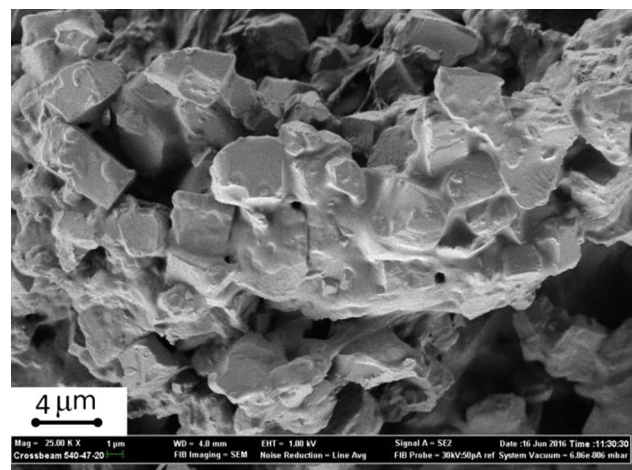
Fig. 3 SEM image of wall detail of an ZF-70 foam

siloxane compounds [30], [33]. If the reaction happens with the external Si–OH groups of PDMS the formation of a covalent Si–O–Si bond, between SAPO-34 zeolite and siloxane compounds, with the formation of water as reaction product, takes place [34]. Analogously, if the reaction occurs with hydride groups of PMHS, the siloxane

Si–O–Si bridge accompanied by hydrogen bubble can be observed [35]. The high chemical interaction between the filler and matrix favors a compact, well-packed composite structure characterized by a stable cellular structure with also good adhesion/cohesion capabilities [28]. This aspect is also identifiable for ZF-70 sample constituted by a low siloxane matrix content. In particular, for this foam batch, due to the large amount of zeolite filler, the zeolite crystals are contiguous, forming a continuous cellular wall structure.

Due to the lower content of zeolite filler, in the ZF-40 foam some local and insulated regions in which the zeolite grains are completely embedded in a wide and large siloxane matrix can be identified (left upper side of the cross section wall in Fig. 2a). These unfilled areas do not influence the water vapor diffusion in the composite foams due to the presence of a large amount of micro-pores in the foam bulk that act as secondary micro-pathways for diffusion processes across the foam cell walls. Furthermore, the presence of PDMS/PMHS silicone film that embeds the zeolite crystals does not act as a barrier to adsorption and desorption processes thanks to its high water vapor permeability (36,000 Barrer) [36, 37].

In Fig. 4, cross-section images of composite foams are reported. A progressive decrease of bubble size dimension is clearly highlighted. At low zeolite content, the mainly interconnected cellular structure can be observed. On the contrary, a mainly closed cell structure can be identified for high zeolite content composite foam. Furthermore, it is possible to notice that for these foams, some local defects triggered in the foam bulk, probably due to a local collapse of higher density foam during the foaming stage [27]. Based on these considerations, a defect-free maximum thickness (DFT) can be identified. The results, obtained for all composite foams, were reported in a graph in Fig. 5. About ZF-40 and ZF-50 foams, a real thickness threshold value has not been detected. Consequently, in the histogram a DFT parameter > 15 mm was conventionally defined. The DFT parameter is progressively reduced as the zeolite filler content increases; the minimum value, 5.0 mm, was observed for ZF-70 foam.

Adsorption properties

The water vapor adsorption isobars of foamed samples were measured by a thermogravimetric dynamic vapor system. First of all, the samples were slowly heated up to 150 °C
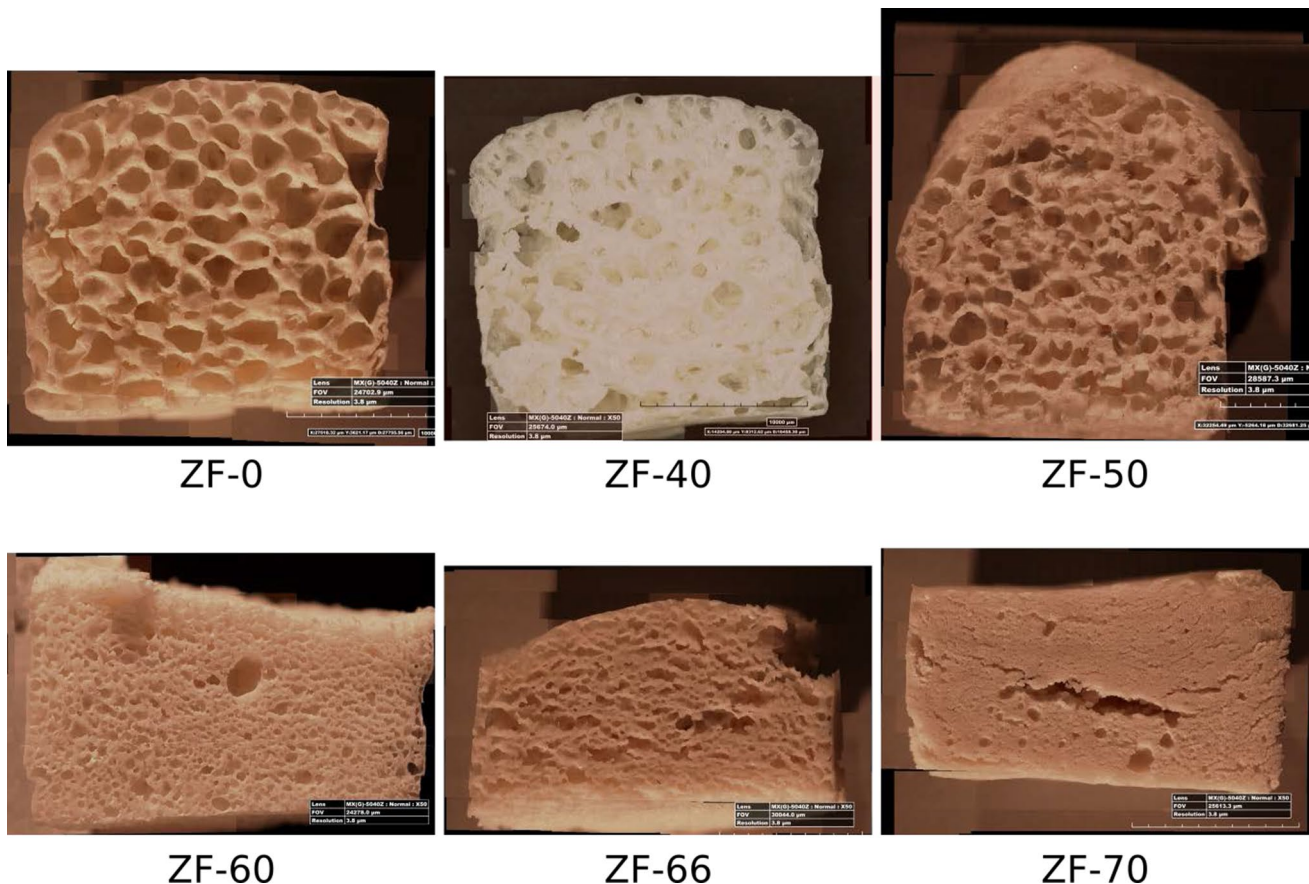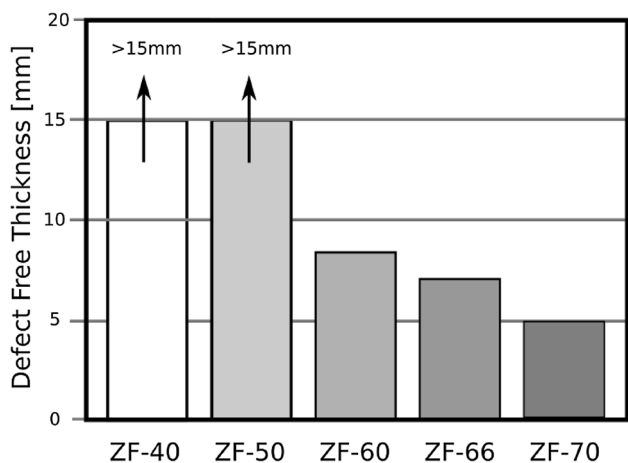

Fig. 4 Cross section image of all foams

Fig. 5 Defect-free maximum thickness (DFT) parameter for all the composite foams

Fig. 6 Water adsorption/desorption isobars at 11 mbar for ZF-70 foam

(heating rate 1 °C/min) and kept at this temperature for about 6 h under continuous evacuation (vacuum level: 10^{-1} Pa), to degas the sample and to calculate its dry weight. Subsequently, a valve connecting the evaporator containing liquid water (maintained at $T = 23$ °C) and the sample chamber was opened. The vapor flows through the system and the vapor (absolute) pressure is kept constant at the set value ($P = 11$ mbar or 42 mbar) by a butterfly valve automatically controlled and by the downstream vacuum pump. The system is controlled by a computer, which also regulates the sample temperature, following the defined temperatures steps (from 23 to 150 °C). At each temperature step, the pressure was kept constant until the sample weight equilibrium was reached.

The water uptake was calculated as:

$$w\left(\frac{g}{g}\right) = \frac{m\left(p_{H_2O}, T_s\right) - m_0}{m_0} \tag{2}$$

where $m(p_{H2O}, T_s)$ (g) represents the weight of the sample at given water vapor pressure and sample temperature, while m_0 (g) is the dry mass of the sample.

Figure 6 shows the adsorption and desorption isobar for ZF-70 reference sample at a water pressure of 11 mbar ($p_{H_2O} = 11$ mbar) in the temperature range 23–150 °C. The $p_{H_2O} = 11$ mbar was specifically selected as it corresponds to evaporation temperature T_{ev} of 7 °C, which represents the typical temperature level for adsorption chiller application, to provide cooling effect. Water uptake curves are characterized by the typical S-shape adsorption trend. An abrupt increase of water uptake can be observed, at about 45 °C, according to the typical SAPO-34 silico-alumino-phosphates behavior. Equilibrium isobars have been measured also in desorption mode, increasing the temperature from room temperature up to 150 °C, without evidence of significant
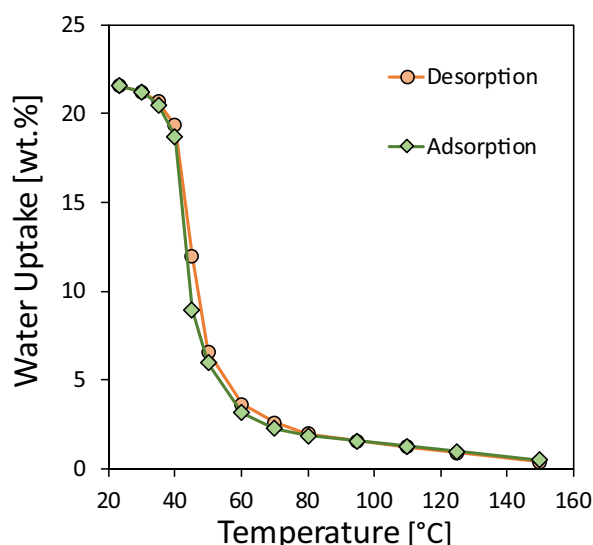
hysteresis phenomenon. This aspect is relevant for adsorption cycles energy performance. Similar trend was evidenced for all the zeolite-based composite foams.

To better highlight the effect of zeolite filler addition on the adsorption performance of the composite foams, Fig. 7 shows the isobars measured in the temperature range of 30–150 °C and at p_{H_2O} of 11 mbar for all zeolite foams formulations. For comparison, the isobar curve of the SAPO-34 powder at the same water vapor pressure was also added. The adsorption curve of Z0-F foam (unfilled foam structure that does not contain SAPO-34 crystals) is not reported
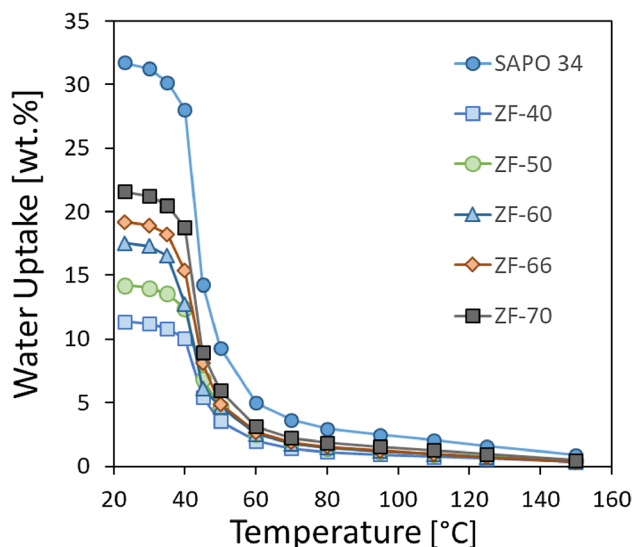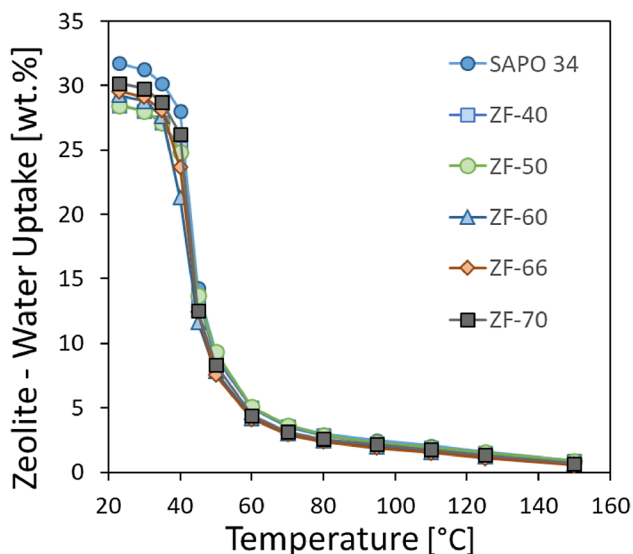

Fig. 7 Water adsorption isobars at 11 mbar for filled zeolite foams and pure zeolite powder

because no adsorption performances were observed in the full temperature range. As expected, isobar curves of Fig. 7 show that the adsorption capacity of the zeolite siloxane foams is lower than pure SAPO-34 powder. The adsorption behavior is consistent with the consideration that the filled zeolite foams are characterized by specific amount of adsorbent material (different quantities of SAPO-34 filler into the foam) and complementary content of inert siloxane matrix, which acts as binder between zeolite grains. However, the maximum adsorption value for the composite foam was observed for ZF-70 batch, where a water uptake above 21.5 wt% is reached. Considering that the pure SAPO-34 zeolite evidenced a maximum water adsorption of 31.7 wt%, this confirms that almost all the zeolite filler loaded inside the composite foam has an active action on the adsorption performances of the foam. This is a further validation of the permeability of the foam structure towards the water vapor flux.

With the purpose to better highlight the adsorption efficiency of the SAPO-34 filler used in the siloxane composite foams, the adsorption curves were normalized respect to the effective adsorbent material amount (zeolite filler) in the foam formulation. In Fig. 8, the obtained adsorption curves of the zeolite foams are reported.

All composites show an adsorption curve quite similar to pure SAPO-34 powder one, confirming that the siloxane matrix does not inhibit the adsorption capacity of the SAPO-34 zeolite filler. Indeed, for instance, for ZF-70 the maximum water uptake was about 30%. Consequently, considering that the maximum water adsorption of zeolite SAPO-34 was about 31.7% it can be concluded that about 95% of the zeolite loaded in the foam structure is actively able to

participate to adsorption and desorption process. PDMS compound, due to its very high water vapor permeability, not influences significantly the adsorption capability of the SAPO-34 filler. The results indicate that zeolite grains have an effective adsorption–desorption behavior independently if located near to bubble surface area or insulated in the foam bulk. This consideration is confirmed by considering the suitable normalized adsorption performances observed for all zeolite-based composite foams.

In this context, another parameter able to elucidate the role of the zeolite filler inside the composite was defined, according to the following formula:

$$FZE_{Ti} = \frac{ZWU_{Foam}}{WU_{SAPO}} \cdot 100 \qquad (3)$$

Where FZE_{Ti} is defined as filled zeolite efficiency, namely the percentage of zeolite, embedded inside the foam, that takes an active role in the adsorption/desorption process at each temperature step. ZWU_{Foam} (wt%) is the water vapor uptake of the composite normalized by the content of the zeolite in each sample and at each temperature (as reported in Fig. 8), while WU_{SAPO} (wt%) is the water vapor uptake of the pure zeolite powder at each temperature (as reported in Fig. 7).

The evolution of FZE parameter at each temperature step for the composite foams is shown in Fig. 9. With low zeolite content foams (ZF-40 and ZF-50), the FZE coefficient is always high throughout the whole temperature range. During the adsorption phase, it can be highlighted that already at high temperatures the zeolite inside the foam has efficiency values higher than 90%. Vice versa, at low

Fig. 8 Normalized Water adsorption isobars at 11 mbar for filled and unfilled zeolite foams
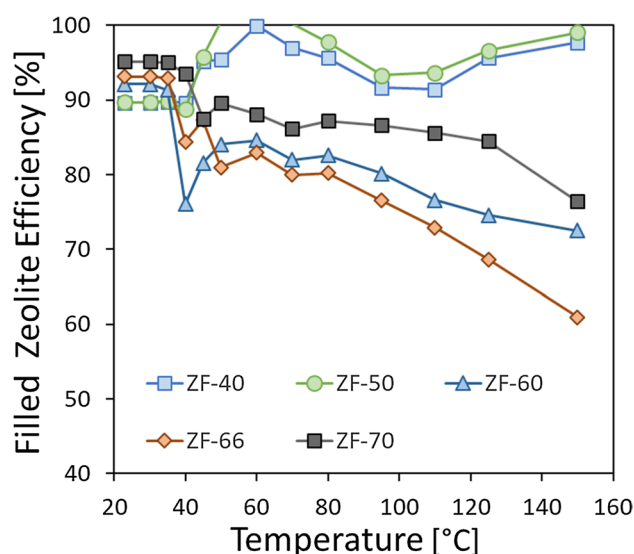
Fig. 9 Filled zeolite efficiency at varying temperature for the composite foams

temperatures, after the adsorption step typical of the SAPO-34 at 45 °C, the FZE efficiency coefficient falls below 90%. Conversely with high zeolite content foams (60%–70 wt%) at high temperatures the filled zeolite has a low efficiency which progressively increases as the temperature decreases until reaching a maximum higher than 90% at low temperatures. A minimum of FZE parameter is observed for ZF-66 sample. Further increasing the zeolite filler content (i.e., ZF-70 foam), a better accessibility of the zeolite through open porosity can be achieved also at high temperature. This behavior can be justified by the presence of micro- and macro-defects on the foam structure (as evidenced in Fig. 4). Therefore, different foams morphology of the foams plays a relevant role in the different adsorption mechanisms.

Low zeolite composite foams are characterized by a large open-cell porous structure. The interconnected porous structure facilitates the vapor access along the whole sample thanks to these large pathways, thus stimulating good adsorption capability also at high temperature. Differently, high zeolite composite foams are characterized by a closed cell porous structure, which allows a flux of the water vapor within the matrix towards the zeolite thanks to the high permeability of the PDMS matrix. This phenomenon is promoted by the presence of micro-channels in the foam structure, which facilitates the formation of preferential paths for vapor permeation. However, in order to allow effective adsorption conditions, lower temperatures are required which energetically favor high water vapor adsorption by the SAPO-34, generating a sufficient driving force for the water vapor flow through the silicone matrix. A bimodal porous distribution characterizes the composite foams: (1) a large porosity, with size cell dimension in the range of millimeters, due to the coalescence and foaming phase occurring during the foam synthesis (2) a nanoscale porosity formed by the packing of zeolite crystal framework. The large porosity in the foamed structure plays a relevant role enhancing the vapor diffusion kinetic throughout the composite sorbent. The water vapor adsorption/desorption phenomena that drive the working cycle is stimulated by the foam nanoscale porosity. This aspect becomes relevant for high zeolite content composite foams where small size cellular foam structure is obtained, therefore, limiting the presence of preferential water vapor pathways along interconnected foam bubbles [27]. However, considering the effective water vapor adsorption, it can be considered plausible that the adsorption mechanism is activated by means of secondary diffusion paths through the siloxane foam, characterized by a good vapor permeability.

Similar considerations can be drawn by analyzing the trend of the adsorption curves for all the composite foams at the vapor pressure $P = 42$ mbar, corresponding to an evaporator temperature of 30 °C. This value was selected representing a typical condensation temperature (i.e., ambient temperature) of an adsorption chiller cycle.

In Fig. 10a, the water vapor uptake normalized for the zeolite filler content is reported. Measurements carried out a $P = 11$ mbar and 42 mbar were compared. In order to increase the readability of the graph only SAPO-34 powder, ZF-40 and ZF-70 foams were chosen for comparison. The composite foams curves have an S-shaped trend quite similar of pristine SAPO-34. Comparing the curves at different vapor pressures, the natural shift of the adsorption jump at higher temperatures is detected. At the same time, there is a slight increase in maximum adsorption capacities which for the SAPO-34 zeolite in powder form is about 2% (from 31.7% at 11 mbat to 33.7% at 42 mbar).
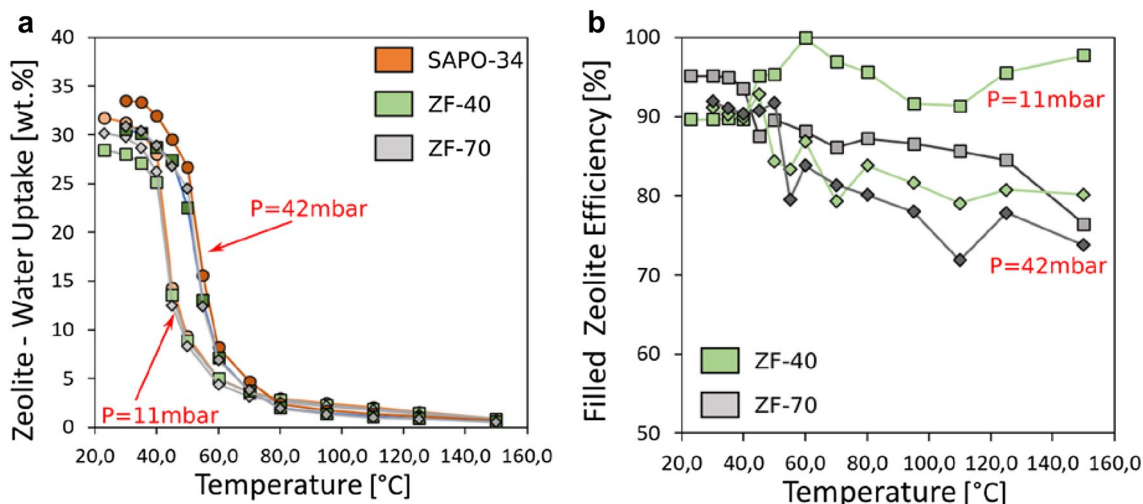
Fig. 10 Water adsorption isobars (**a**) and Filled zeolite efficiency (**b**) for filled zeolite foams (ZF-40 and ZF-70) and pure zeolite powder at $P = 11$ mbar and $P = 42$ mbar
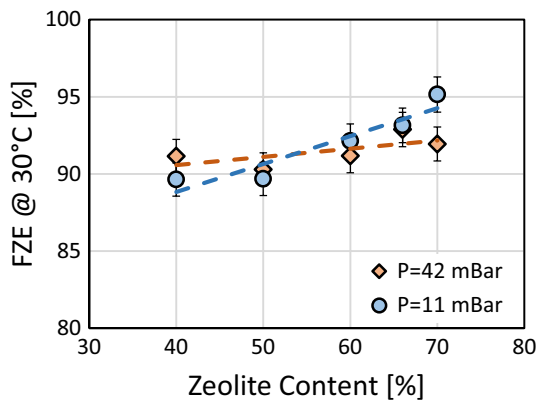
Fig. 11 Filled zeolite efficiency parameter at 30 °C vs zeolite content at $P = 11$ mbar and $P = 42$ mbar

Further information can be obtained by analyzing the evolution of the FZE coefficient for each temperature step and at the two investigated water vapor pressures (Fig. 10b). Analyzing the trend of curves at P = 42 mbar, it is evident that, at high temperatures, the ZF-40 at 42 mbar curve has a higher efficiency than the ZF-70 at 42 mbar. This latter batch, in particular, showed an efficiency lower than 80% up to about 100 °C. Afterwards, progressively, with the reduction of temperature, there is a significant increase in the adsorption efficiency of the zeolite inside the foam, until reaching a suitable FZE coefficient, above 90%, at s. This behavior is quite similar from what was found for the tests performed at $P = 11$ mbar, and discussed in Fig. 9. Comparing $P = 11$ mbar and $P = 42$ mbar FZE parameters, a slight difference can be evidenced. Although in this range of temperature, the instrument sensitivity and the water vapor adsorption of zeolite filler are very low, thus inducing not statistically significant this range of temperature.

Figure 11 compares the efficiency at 30 °C of zeolite filler in the composite foams (FZE@30 °C) for adsorption tests at $P = 11$ mbar and $P = 42$ mbar. For each specific water pressure, a quite linear relationship between FZE parameter and zeolite content was observed. Regardless of the set water vapor pressure, the composite foams with a higher zeolite content have shown a very similar efficiency, with values close to 92% of FZE parameter at 30 °C. Differently, this parameter decreases when the zeolite content in the composite foam is lower. In particular, the results of isobars at $P = 11$ mbar, differently from $P = 42$ mbar, showed a higher dependence of FZE from filler content as confirmed by higher slope of linear trend line for $P = 11$ mbar data. The filled zeolite efficiency parameter for ZF-40 foam varies from 91.1 to 89.6% at $P = 42$ mbar and $P = 11$ mbar, respectively. Conversely, for ZF-70, the FZE parameter varies from 91.9 to 95.1% at $P = 42$ mbar and $P = 11$ mbar, respectively.

Preliminary stability tests, not reported in this work, on the composite foam up to 1500 adsorptions/desorption cycles (T_{ads} 30 °C, T_{des} 95 °C P_{ev} 12 mbar) were performed without evidence of any performance degradation. Consequently, composite adsorbents constituted by zeolite–PDMS foams could identify a new adsorbent material with promising prospects in the optimization process of adsorbent beds AHP systems.

Thermodynamic analysis

Starting from the above-reported experimental activity, the thermodynamic analysis of the proposed foam technology was performed. The idea was to compare the thermodynamic efficiency, in terms of cooling COP, of a typical adsorber solution based on loose adsorbent grains inside an aluminum finned-flat tube heat exchanger (HEX) against the proposed foam compositions. According to the isobars experimentally measured, the

Table 2 Reference data for the aluminum finned-flat tube HEX

Reference HEX	Dimensions (cm)	Overall volume (dm³)	Metal mass (kg)	Heat transfer surface (m²)	Ratio empty volume/overall volume, α (m³ m⁻³)
	23.5 × 15.7 × 2.2	1.0	0.51	0.94	0.6

selected reference cycle for air conditioning application was $T_{des} = 90\ °C$; $T_{ads} = T_{cond} = 30\ °C$; $T_{ev} = 7\ °C$.

The reference data for the HEX were taken from the one proposed in [16] and summarized in Table 2.

The calculations were carried out adapting the thermodynamic model reported in [5]. The cooling COP was defined as:

$$COP = \frac{Q_{cool}}{Q_{des}} \qquad (4)$$

where Q_{cool} (kJ) represents the cooling energy provided by the reference adsorber and Q_{des} (kJ) is the heating energy spent for the adsorption cooling cycle.

These values are calculated as follows:

$$Q_{cool} = L(T_{ev}) \Delta w \rho_{sol} \alpha V_{HEX} \gamma \qquad (5)$$

$$Q_{des} = \big((cp_{eq}(w_{ave}) + cp_{Al} r)(T_{des} - T_{ads}) + \Delta H_{ads} \Delta w \big) \\ \big(\Delta w \rho_{sol} \alpha V_{HEX} \gamma \big) \qquad (6)$$

where:

– $L(T_{ev})$ (kJ kg^{-1}) is the latent heat of evaporation of water at evaporation temperature,
– Δw (kg kg^{-1}) is the water vapor exchange between adsorption and desorption,
– ρ_{sol} (kg m^{-3}) is the density of the solid (i.e., SAPO-34 pellets or foam),
– α (m^3 m^{-3}) is the ratio between empty volume and overall volume of the HEX,
– V_{HEX} (m^3) is the overall volume of the HEX;
– γ (–) is the package density of the solid adsorbent inside the HEX;
– $cp_{eq}(w_{ave})$ (kJ kg^{-1} K^{-1}) is the equivalent specific heat calculated at an average uptake value between adsorption and desorption, calculated as reported by [38];
– cp_{Al} (kJ kg^{-1} K^{-1}) is the specific heat of aluminum;
– r (kg kg^{-1}) is the metal to solid mass ratio;
– T_{des} (°C) is the desorption temperature;

– T_{ads} (°C) is the adsorption temperature;
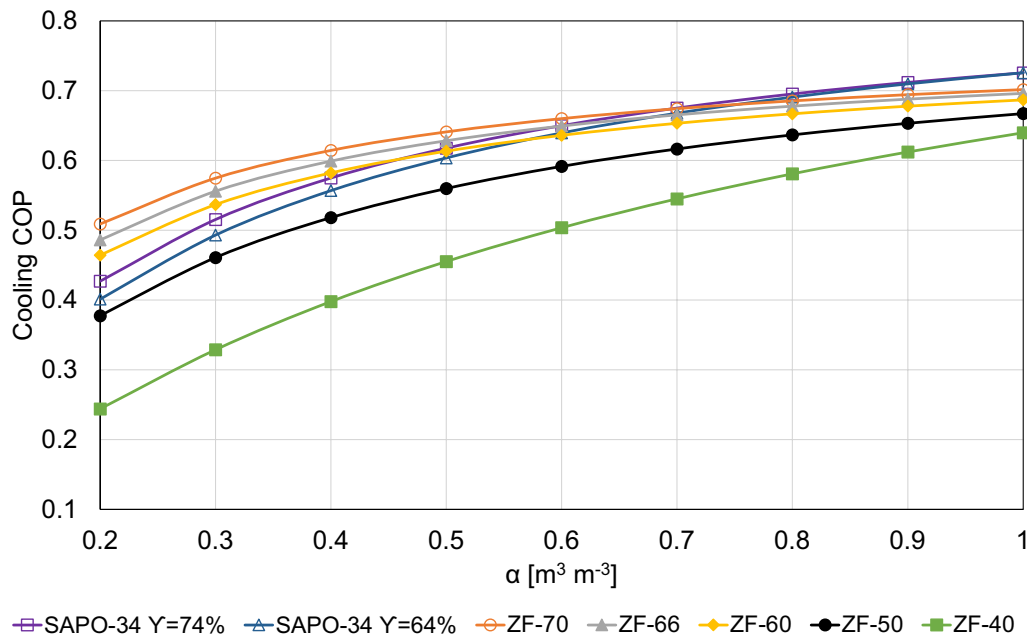– ΔH_{ads} (kJ kg^{-1}) is the average heat of adsorption of the SAPO-34.

The parameters' values are summarized in Table 3.

The parameter γ, representing the package density of the solid between the HEX fins, varies passing from the loose grains configuration to the composite foam. Indeed, for the latter, this parameter is equal to 1.0, since the whole volume can be filled with the foam itself. On the contrary, the packing density of SAPO-34 grains, assumed as spheres, is not a uniquely defined problem. Indeed, it is known that the theoretical maximum achievable packing density is about 0.74, but typical values obtained randomly dispersing monosized spheres in a confined volume are in the range of 0.64 [42]. Accordingly, the cooling COP was calculated for two loose grains configurations (with γ equal to 0.74 and 0.64) and for five foam configurations (i.e., ZF-70, ZF-66, ZF-60, ZF-50 and ZF-40).

Furthermore, the calculations were parametrized as function of the ratio between empty volume and overall volume of the HEX, α. This parameter varies by varying the fin pitch and the fin thickness of the HEX. The lower is the fin pitch (or the higher is the fin thickness) the lower is α. The reference value α for the identified HEX is 0.6, as reported in Table 2. For the parametric analysis, α was varied from 0.2 (i.e., high fin density HEX) up to 1.0 (i.e., ideal condition where no metal is present). The obtained results are summarized in Fig. 12.

Analyzing the achieved results, the first comment, related to the loose grains packing density is that, in the range of α typical of these HEXs (i.e., between 0.7 and 0.4), the difference in COP is ranging between 1 and 3%, comparing $\gamma = 0.74$ and $\gamma = 0.64$. In the same α range, comparing the most effective foam solution (ZF-70) with the high packing density loose grain solution, the foam one is always more efficient, reaching a COP increase of 7% when $\alpha = 0.4$. The beneficial effect of the foam on the adsorber efficiency is even more pronounced for low α values (i.e., below 0.4). On the contrary, the loose grain solution is more efficient when the empty HEX volume is higher. This behavior can be justified by the fact that, when there is a big available volume, the effect of the packing density is less relevant.

These results confirm the promising features of the composite foam technology. Indeed, since the recent R&D activities in the adsorption heat pump field are focusing on the enhancement of the heat transfer surface area, in order to optimize the heat transfer efficiency of adsorbers, it can be argued that the composite foam will be able to offer both better energy efficiency and power density if compared to the state-of-the-art loose grains configurations.

Table 3 Values of the parameters employed for the thermodynamic models

Parameter	Value	References
$L(7\ °C)$ (kJ kg^{-1})	2485	[39]
ρ_{sol} (kg m^{-3}) SAPO-34 grain	600	[41]
ρ_{sol} (kg m^{-3}) ZF-70	1020	[27]
ρ_{sol} (kg m^{-3}) ZF-66	940	[27]
ρ_{sol} (kg m^{-3}) ZF-60	920	[27]
ρ_{sol} (kg m^{-3}) ZF-50	670	[27]
ρ_{sol} (kg m^{-3}) ZF-40	380	[27]
$cp_{SAPO-34}$ (kJ kg^{-1} K^{-1})	0.8	[38]
cp_{Al} (kJ kg^{-1} K^{-1})	0.9	[39]
ΔH_{ads} (kJ kg^{-1})	2900	[40]

Fig. 12 Cooling COP as a function of the ratio between available volume and overall volume of the HEX, calculated for two loose grains and composite foams configurations

Conclusions

Morphological analysis coupled with adsorption performances and thermodynamic analysis of innovative composite SAPO-34/silicone foams was performed. The obtained results highlighted that the macro-cellular structure of the composite foam is influenced by the zeolite content. In particular, open and closed cell structure was observed for large or low zeolite composite foams, respectively. Anyway, in all samples, zeolite was interconnected, well packed and embedded effectively in the silicone matrix. However, some foaming defects were observed for ZF-60 and ZF70 samples, as highlighted by a defect free maximum thickness (DFT) parameter of 7.1 and 5.0 mm, respectively.

Adsorption/desorption tests evidenced that the composite foams have very effective adsorption performances. The addition of silicone matrix only slightly affects the porous structure of the pure zeolite that preserved good adsorption capabilities. Tests, performed at $P = 11$ mbar and 42 mbar, indicated a filled zeolite efficiency parameter at 30 °C above 85% for all foam formulations. Best results were observed for ZF-70 samples where a filled zeolite efficiency parameter of about 92% was calculated. Additionally, a simple thermodynamic analysis based on energy balances demonstrated that the proposed foam technology can guarantee cooling COP up to 7% higher than that estimated for the conventional configuration loose adsorbent grains inside aluminum finned-flat tube HEX. This highlights that this class of adsorbent composite materials could represent an effective and suitable alternative to the other conventional ways to embed zeolite inside HEXs to realize adsorbers for AHP applications (e.g., coating, direct synthesis, loose grains).

Future activities will be dedicated to the evaluation of the physical and mechanical stability of the composite foams operated under real boundary conditions.

References

1. Meunier, F.: Adsorption heat powered heat pumps. Appl. Therm. Eng. **61**, 830–836 (2013). https://doi.org/10.1016/j.applthermaleng.2013.04.050
2. Aristov, Y.I.: Optimal adsorbent for adsorptive heat transformers: dynamic considerations. Int. J. Refrig. **32**, 675–686 (2009). https://doi.org/10.1016/j.ijrefrig.2009.01.022
3. Aristov, Y.: Concept of adsorbent optimal for adsorptive cooling/heating. Appl. Therm. Eng. **72**, 166–175 (2014). https://doi.org/10.1016/j.applthermaleng.2014.04.077
4. Aristov, Y.I.: Challenging offers of material science for adsorption heat transformation: a review. Appl. Therm. Eng. **50**, 1610–1618 (2013). https://doi.org/10.1016/j.applthermaleng.2011.09.003

5. Freni, A., Maggio, G., Sapienza, A., Frazzica, A., Restuccia, G., Vasta, S.: Comparative analysis of promising adsorbent/adsorbate pairs for adsorptive heat pumping, air conditioning and refrigeration. Appl. Therm. Eng. **104**, 85–95 (2016). https://doi.org/10.1016/j.applthermaleng.2016.05.036

6. Fong, K.F., Lee, C.K.: Impact of adsorbent characteristics on performance of solid desiccant wheel. Energy. **144**, 1003–1012 (2018). https://doi.org/10.1016/j.energy.2017.12.113

7. De Lange, M.F., Verouden, K.J.F.M., Vlugt, T.J.H., Gascon, J., Kapteijn, F.: Adsorption-driven heat pumps: the potential of metal-organic frameworks. Chem. Rev. **115**, 12205–12250 (2015). https://doi.org/10.1021/acs.chemrev.5b00059

8. Gordeeva, L.G., Aristov, Y.I.: Composites "salt inside porous matrix" for adsorption heat transformation: a current state-of-the-art and new trends. Int. J. Low. Carbon. Technol. **7**, 288–302 (2012). https://doi.org/10.1093/ijlct/cts050

9. Li, X., Narayanan, S., Michaelis, V.K., Ong, T.C., Keeler, E.G., Kim, H., McKay, I.S., Griffin, R.G., Wang, E.N.: Zeolite Y adsorbents with high vapor uptake capacity and robust cycling stability for potential applications in advanced adsorption heat pumps. Microporous. Mesoporous. Mater. **201**, 151–159 (2015). https://doi.org/10.1016/j.micromeso.2014.09.012

10. Henninger, S.K., Ernst, S.J., Gordeeva, L., Bendix, P., Froehlich, D., Grekova, A.D., Bonaccorsi, L., Aristov, Y., Jaenchen, J.: New materials for adsorption heat transformation and storage. Renew. Energy. **110**, 59–68 (2017). https://doi.org/10.1016/j.renene.2016.08.041

11. Demir, H., Mobedi, M., Ülkü, S.: A review on adsorption heat pump: problems and solutions. Renew. Sustain. Energy. Rev. **12**, 2381–2403 (2008). https://doi.org/10.1016/j.rser.2007.06.005

12. Bonaccorsi, L., Calabrese, L., Freni, A., Proverbio, E., Restuccia, G.: Zeolites direct synthesis on heat exchangers for adsorption heat pumps. Appl. Therm. Eng. **50**, 1590–1595 (2013). https://doi.org/10.1016/j.applthermaleng.2011.10.028

13. Bauer, J., Herrmann, R., Mittelbach, W., Schwieger, W.: Zeolite/aluminum composite adsorbents for application in adsorption refrigeration. Int. J. Energy. Res. **33**, 1233–1249 (2009). https://doi.org/10.1002/er.1611

14. Bonaccorsi, L., Calabrese, L., Proverbio, E.: Low temperature single-step synthesis of zeolite Y coatings on aluminium substrates. Microporous. Mesoporous. Mater. **144**, 40–45 (2011). https://doi.org/10.1016/j.micromeso.2011.04.014

15. Schnabel, L., Tatlier, M., Schmidt, F., Erdem-Senatalar, A.: Adsorption kinetics of zeolite coatings directly crystallized on metal supports for heat pump applications (adsorption kinetics of zeolite coatings). Appl. Therm. Eng. **30**, 1409–1416 (2010). https://doi.org/10.1016/j.applthermaleng.2010.02.030

16. Freni, A., Bonaccorsi, L., Calabrese, L., Caprì, A., Frazzica, A., Sapienza, A.: SAPO-34 coated adsorbent heat exchanger for adsorption chillers. Appl. Therm. Eng. **82**, 1–7 (2015). https://doi.org/10.1016/j.applthermaleng.2015.02.052

17. Freni, A., Russo, F., Vasta, S., Tokarev, M., Aristov, Y.I., Restuccia, G.: An advanced solid sorption chiller using SWS-1L. Appl. Therm. Eng. **27**, 2200–2204 (2007). https://doi.org/10.1016/j.applthermaleng.2005.07.023

18. Freni, A., Frazzica, A., Dawoud, B., Chmielewski, S., Calabrese, L., Bonaccorsi, L.: Adsorbent coatings for heat pumping applications: verification of hydrothermal and mechanical stabilities. Appl. Therm. Eng. **50**, 1658–1663 (2013). https://doi.org/10.1016/j.applthermaleng.2011.07.010

19. Calabrese, L., Bonaccorsi, L., Caprì, A., Proverbio, E.: Electrochemical behavior of hydrophobic silane–zeolite coatings for corrosion protection of aluminum substrate. J. Coatings. Technol. Res. **11**, 883–898 (2014). https://doi.org/10.1007/s11998-014-9597-4

20. Calabrese, L., Bonaccorsi, L., Caprì, A., Proverbio, E.: Enhancement of the mechanical properties of a zeolite based composite coating on an aluminum substrate by silane matrix modification. Ind. Eng. Chem. Res. **55**, 6952–6960 (2016). https://doi.org/10.1021/acs.iecr.6b00844

21. Lee, Y.-J., Lee, J.S., Park, Y.S., Yoon, K.B.: Synthesis of large monolithic zeolite foams with variable macropore architectures. Adv. Mater. **13**, 1259 (2001). https://doi.org/10.1002/1521-4095(200108)13:16%3c1259:AID-ADMA1259%3e3.0.CO;2-U

22. Hu, P., Yao, J.J., Chen, Z.S.: Analysis for composite zeolite/foam aluminum-water mass recovery adsorption refrigeration system driven by engine exhaust heat. Energy. Convers. Manag. **50**, 255–261 (2009). https://doi.org/10.1016/j.enconman.2008.09.022

23. Bonaccorsi, L., Calabrese, L., Freni, A., Proverbio, E.: Hydrothermal and microwave synthesis of SAPO (CHA) zeolites on aluminium foams for heat pumping applications. Microporous. Mesoporous. Mater. **167**, 30–37 (2013). https://doi.org/10.1016/j.micromeso.2012.06.006

24. Freni, A., Bonaccorsi, L., Proverbio, E., Maggio, G., Restuccia, G.: Zeolite synthesised on copper foam for adsorption chillers: a mathematical model. Microporous. Mesoporous. Mater. **120**, 402–409 (2009). https://doi.org/10.1016/j.micromeso.2008.12.011

25. Bonaccorsi, L., Bruzzaniti, P., Calabrese, L., Freni, A., Proverbio, E., Restuccia, G.: Synthesis of SAPO-34 on graphite foams for adsorber heat exchangers. Appl. Therm. Eng. **61**, 848–852 (2013). https://doi.org/10.1016/j.applthermaleng.2013.04.053

26. Calabrese, L., Bonaccorsi, L., Freni, A., Proverbio, E.: Synthesis of SAPO-34 zeolite filled macrocellular foams for adsorption heat pump applications: a preliminary study. Appl. Therm. Eng. **124**, 1312 (2017). https://doi.org/10.1016/j.applthermaleng.2017.06.121

27. Calabrese, L., Bonaccorsi, L., Bruzzaniti, P., Freni, A., Proverbio, E.: Morphological and functional aspects of zeolite filled siloxane composite foams. J. Appl. Polym. Sci. **135**, 45683 (2018). https://doi.org/10.1002/app.45683

28. Calabrese, L., Bonaccorsi, L., Bruzzaniti, P., Gullì, G., Freni, A., Proverbio, E.: Zeolite filled siloxane composite foams: compression property. J. Appl. Polym. Sci. **135**, 46145 (2018). https://doi.org/10.1002/app.46145

29. Bonaccorsi, L.M., Calabrese, L., Caprì, A., Proverbio, E., Bruzzaniti, P., Freni, A., Frazzica, A., Restuccia, G., Sapienza, A., Vasta, S.: Metodo per produrre una schiuma zeolitica adsorbente, schiuma così ottenuta e sue applicazioni, 102015000044739 Patent, (2015)

30. Calabrese, L., Bonaccorsi, L., Freni, A., Proverbio, E.: Silicone composite foams for adsorption heat pump applications. Sustain. Mater. Technol. **12**, 27–34 (2017). https://doi.org/10.1016/j.susmat.2017.04.002

31. Chruściel, J.J., Leśniak, E.: Preparation of flexible, self-extinguishing silicone foams. J. Appl. Polym. Sci. **119**, 1696–1703 (2011). https://doi.org/10.1002/app.32852

32. Jawhar, M.-C.D., Blanc, D., Chaumont, P., Cassagnau, P.: Study of the coalescence mechanisms during silicone foaming. Macromol. Mater. Eng. **299**, 336–343 (2013). https://doi.org/10.1002/mame.201300142

33. Calabrese, L., Bonaccorsi, L., Caprì, A., Proverbio, E.: Adhesion aspects of hydrophobic silane zeolite coatings for corrosion protection of aluminium substrate. Prog. Org. Coat. **77**, 1341–1350 (2014). https://doi.org/10.1016/j.porgcoat.2014.04.025

34. Zhang, H., Lamb, R.N., Jones, A.W.: Durable superhydrophobic coating, WO2004090065 patent (2004)

35. Lin, J., Chen, H., Yuan, Y., Ji, Y.: Mechanochemically conjugated PMHS/nano-SiO_2 hybrid and subsequent optimum

grafting density study. Appl. Surf. Sci. **257**, 9024–9032 (2011). https://doi.org/10.1016/j.apsusc.2011.05.093

36. Robb, W.L.: Thin silicon membranes. Their permeation properties and some applications. Ann. N. Y. Acad. Sci. **146**, 119–137 (1968). https://doi.org/10.1111/j.1749-6632.1968.tb20277.x

37. Wai Lin, S., Valera Lamas, S.: Air dehydration by permeation through dimethylpolysiloxane/polysulfone membrane. J. Mex. Chem. Soc. **55**, 42–50 (2011)

38. Santori, G., Frazzica, A., Freni, A., Galieni, M., Bonaccorsi, L., Polonara, F., Restuccia, G.: Optimization and testing on an adsorption dishwasher. Energy. **50**, 170–176 (2013). https://doi.org/10.1016/J.ENERGY.2012.11.031

39. Cengel, Y.A., Boles, M.A.: Thermodynamics: an engineering approach. Mac Graw Hill, New York (2015)

40. Bales, C., Gantenbein, P., Hauer, A., Henning, H.-M., Jaenig, D., Kerskes, H., Nuñez, T., Visscher, K.: Thermal properties of materials for thermo-chemical storage of solar heat: report B2 of subtask B. IEA-SHC,Task 32, report (2005)

41. Erdogan, M., Graf, S., Bau, U., Lanzerath, F., Bardow, A.: Simple two-step assessment of novel adsorbents for drying: the trade-off between adsorber size and drying time. Appl. Therm. Eng. **125**, 1075–1082 (2017). https://doi.org/10.1016/J.APPLTHERMALENG.2017.07.014

42. Reimann, J., Vicente, J., Brun, E., Ferrero, C., Gan, Y., Rack, A.: X-ray tomography investigations of mono-sized sphere packing structures in cylindrical containers. Powder Technol. **318**, 471–483 (2017). https://doi.org/10.1016/j.powtec.2017.05.033